Novel High-Performance Polymer Memory Devices Containing $(OMe)_2$Tetraphenyl-*p*-phenylenediamine Moieties

CHIH-JUNG CHEN,[1] HUNG-JU YEN,[1] WEN-CHANG CHEN,[1,2] GUEY-SHENG LIOU[1]

[1]Functional Polymeric Materials Laboratory, Institute of Polymer Science and Engineering, National Taiwan University, 1 Roosevelt Road, 4th Sec., Taipei 10617, Taiwan

[2]Department of Chemical Engineering, National Taiwan University, 1 Roosevelt Road, 4th Sec., Taipei 10617, Taiwan

Received 28 April 2011; accepted 24 May 2011
DOI: 10.1002/pola.24807
Published online 20 June 2011 in Wiley Online Library (wileyonlinelibrary.com).

ABSTRACT: The functional polyimide **$(OMe)_2$TPPA-6FPI** (**PI**) and the polyamide **$(OMe)_2$TPPA-6FPA** (**PA**) consisting of electron-donating *N,N′*-bis(4-aminophenyl)-*N,N′*-di(4-methoxylphenyl)1,4-phenylenediamine [$(OMe)_2$TPPA-diamine] for memory application were prepared in this study. These polyimide and polyamide memory devices were fabricated with the sandwich configuration of indium tin oxide (ITO)/polymer/Al, and could be switched from the initial low-conductivity (OFF) state to the high-conductivity (ON) state with high ON/OFF current ratios of 10^7 and 10^9, respectively. **PI** exhibited dynamic random access memory (DRAM) performance, whereas **PA** showed static random access memory (SRAM) behavior. To get more insight into the memory behaviors of these two different types of polymer memory devices, molecular simulation on the basic unit was carried out. Furthermore, the differences of highest occupied molecular orbital (HOMO) energy level, lowest unoccupied molecular orbital (LUMO) charge density isosurfaces, dipole moment, and linkage conformation between **PI** and **PA** were found to affect the volatile memory behavior. Both polymer memory devices revealed excellent stability with long operation time of 10^4 s at continuous applied voltage of -2 V. The effect of polymer thickness on the volatile memory behavior of **PA** was also investigated in this study. © 2011 Wiley Periodicals, Inc. J Polym Sci Part A: Polym Chem 49: 3709–3718, 2011

KEYWORDS: bistability; DRAM; functionalization of polymers; high performance polymers; memory; polyamides; polyimides; SRAM

INTRODUCTION Over the years, the use of polymeric materials in electronic devices has attracted significant attention, such as light-emitting devices,[1] transistors,[2] solar cells,[3] and memory devices.[4] Because of the advantages of rich structural flexibility, low-cost, solution processability, and three-dimensional stacking capability,[5] electrically bistable resistive switching polymeric materials have great merits over inorganic silicon- and metal-oxide-based memory materials. When compared with the traditional inorganic memory materials, polymeric memory materials store information in the form of high (ON) and low (OFF) current state in place of the amount of charges stored in a cell in silicon devices. In the starting stage of polymer memory applications, polymers were used as polyelectrolytes[6] and matrices in a doped system.[4(f),7] To advance the function of polymers for memory devices further, the design and synthesis of the polymers with specific structures that can provide expected memory properties within single polymer chain are an important and crucial issue.

Among all the studied polymer systems, polyimides are promising candidates for memory device applications.[8] Comparing with polyimides, most of other memory polymer materials have aliphatic hydrocarbon backbones that exhibit low-dimensional stability or high OFF current.[9] Polyimide is an insulating material which is advantageous in decreasing OFF current. Polyimides containing both electron donor and acceptor moieties within a repeating unit, which can contribute electronic transition between the ground and excited states and also show excellent physical and chemical properties. The introduction of triphenylamide (TPA) group into polymer could increase the solubility of polymer and enhance the solution processability.[10] The TPA-based polyimides 6F-TPA PI[8(a)] used by Kang and coworkers demonstrated electrical switching behavior and indicated as volatile dynamic random access memory (DRAM).[8(b)] Then, a series of TPA-based polyimides with different substituted groups were prepared and used to fabricate memory devices, such as 4-hydroxy-substituted TPA-based polyimide (6F-HTPA PI) derived from 4,4′-amino-4″-hydroxy-triphenylamine and 2,2-bis(3,4-dicarboxyphenyl)hexafluoropropane dianhydride (6FDA) was reported and revealed significant different memory properties from 6F-TPA PI. The polyimide with the OH-substituted TPA did not show DRAM but write-once-read-many-times (WORM) properties.[8(e)] Meanwhile, Ree and coworkers fabricated polymer memory device based

Additional Supporting Information may be found in the online version of this article. Correspondence to: G.-S. Liou (E-mail: gsliou@ntu.edu.tw)

on 4-(*N*,*N*-diphenylamine)-substituted TPA-based polyimide (6F-2TPA PI) prepared from *N*,*N*-bis(4-aminophenyl)-*N*′,*N*′-diphenyl-1,4-phenylenediamine and dianhydride 6FDA. The polyimide (6F-2TPA PI) exhibited nonvolatile WORM and volatile DRAM characteristics depending on the thickness of polymer films.[8(g)] The diverse memory properties of TPA-based polyimides with different substituted groups imply the importance of electron-donating moieties. Therefore, the relationship between the electron donor structures and memory device characteristics requires further exploration. In this study, $(OMe)_2$TPPA moiety was chosen as an electron donor. Comparing to 2TPA, $(OMe)_2$TPPA has two electroactive nitrogen atoms in the main chain with substituted electro-donating methoxy groups that results in not only higher highest occupied molecular orbital (HOMO) energy level which has been considered as a contribution for the lower switching-on voltage but also improvements of device lifetime due to the stabilized cationic radical after oxidation. Besides the electron donor structures effect, the difference of electrical switching behavior between DRAM and static random access memory (SRAM) can also be induced by introduction of different linkage groups between the electron donor and the electron acceptor moieties.[8(i,k)] The conformational changes between the donor and acceptor moiety induced by charge-transfer (CT) increase the torsional displacement and produce a potential energy barrier for the CT complex to the back electron transfer. As a result, the retention time for the polymer memory device maintaining at ON state should be longer after removing the applying electric field. This phenomenon could be attributed to the longer relaxation time needed from the excited state to ground state of the reverse charge-transfer complex; thus, the obtaining polymer memory device should be SRAM type memory behavior. In addition to the linkage difference, the dipole moment also manifested significant effect on memory properties. According to previous literature, the higher dipole moment led to a more stable CT structure and increased ON state retention time of memory device after removing applied power.[4(c),8(j,k)] With the dipole moment increasing, polymer memory properties can transit from DRAM to SRAM and even become WORM type or flash type memory behavior.

In addition to polyimides, wholly aromatic polyamides were also characterized as highly thermally stable polymers with a favorable balance of physical and chemical properties. In our previous study, TPA or tetraphenyl-substituted *p*-phenylenediamine (TPPA)-based polyamides showed excellent electrochemical stability.[11] Besides, the difference of linkages, HOMO and lowest unoccupied molecular orbital (LUMO) energy levels between polyamides and polyimides should be expected to reveal different memory characteristics, such as the higher HOMO energy level of polyamides which may be predicted to have the lower operation voltage. However, to the best of our knowledge, the polymeric memory materials based on aromatic polyamides have not been reported to date. Therefore, we reported the new functional polyimide **$(OMe)_2$TPPA-6FPI** (**PI**) derived from electron-donating *N*,*N*′-bis(4-aminophenyl)-*N*,*N*′-di(4-methoxylphenyl)1,4-phenylenediamine [$(OMe)_2$TPPA-diamine] and 4,4′-(hexafluoroisopropylidene)diphthalic anhydride (6FDA) as the acceptor. In addition, the polyamide **$(OMe)_2$TPPA-6FPA** (**PA**) consisting of electron-donating $(OMe)_2$TPPA-diamine moieties and 2,2′-bis(4-carboxyphenyl)hexafluoropropane (6FDC) was also prepared for detailed comparison study. The obtained $(OMe)_2$TPPA-containing polyimide and polyamide are solution-processable polymers and could be readily cast into a smooth film layer by spin coating. These polymer memory devices were fabricated with the sandwich configuration of ITO/polymer/Al, and the memory properties were investigated by *I*–*V* measurements. The difference of dipole moment, HOMO energy level, LUMO charge density isosurfaces, and linkage conformation between **PI** and **PA** was found to affect the volatile memory behavior. To investigate switching mechanism of the memory devices further, molecular simulation on the basic unit was carried out by DFT/B3LYP/6-31G(d) with the Gaussian 09 program and the effect of polymer thickness on the volatile memory behavior of **PA** were also described in this study.

EXPERIMENTAL

Materials

N,*N*′-Bis(4-aminophenyl)-*N*,*N*′-di(4-methoxylphenyl)-1,4-phenylenediamine (**1**) was synthesized according to a previously reported procedure.[11(b)] An electroactive TPPA-based aromatic polyamide **$(OMe)_2$TPPA-6FPA** (**PA**) was prepared from the diamine monomer (**1**) with aromatic dicarboxylic acid, 2,2′-bis(4-carboxyphenyl)hexafluoropropane (6FDC; **2**), via the phosphorylation polyamidation.[11(b)] 2,2-Bis(3,4-dicarboxyphenyl)hexafluoropropane dianhydride (6FDA, **3**; Chriskev) was purified by vacuum sublimation. Tetrabutylammonium perchlorate (TBAP; Acros) was recrystallized twice by ethyl acetate under nitrogen atmosphere and then dried *in vacuo* before use. All other reagents were used as received from commercial sources.

Preparation of PI by Two-Step Method via Chemical Imidization Reaction

To a solution of 0.51 g (1.01 mmol) of diamine (**1**) in 2.8 mL of *N*-methyl-2-pyrrolidinone (NMP), 0.45 g (1.01 mmol) of dianhydride 6FDA (**3**) was added in one portion. The mixture was stirred overnight (*ca*. 12 h) at room temperature to afford a viscous poly(amic acid) solution. The poly(amic acid) was subsequently converted to polyimide via a chemical imidization process by the addition of 1.0 mL of pyridine and 2.0 mL of acetic anhydride; then, the mixture was heated at 120 °C for 4 h to complete imidization. The resulting polymer solution was poured into 300 mL of methanol giving a fibrous precipitate washed thoroughly with methanol. The weight-average molecular weights (M_w) and polydispersity index of **PI** was 129,300 and 2.06, respectively, relative to polystyrene standards.

Polymer Properties Measurements

Fourier transform infrared (FTIR) spectra were recorded on a PerkinElmer Spectrum 100 Model FTIR spectrometer. ^{1}H NMR spectra were measured on a Bruker AC-300 MHz

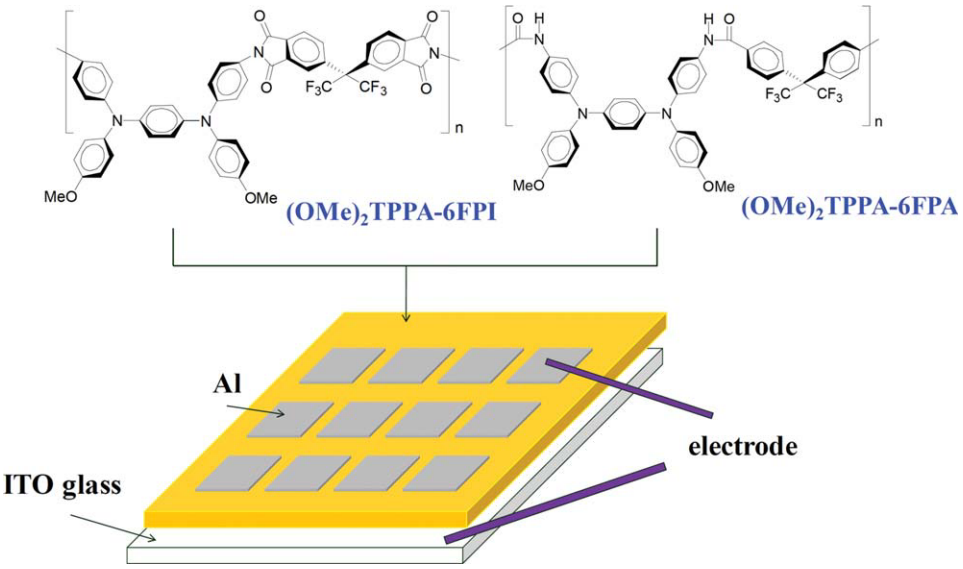

FIGURE 1 Molecular structures of **$(OMe)_2$TPPA-6FPI** and **$(OMe)_2$TPPA-6FPA**, and schematic diagram of the memory device consisting of a polymer thin film sandwiched between an ITO bottom electrode and an Al top electrode. [Color figure can be viewed in the online issue, which is available at wileyonlinelibrary.com.]

spectrometer in DMSO-d_6, using tetramethylsilane as an internal reference, and peak multiplicity was reported as follows: s, singlet; d, doublet; and m, multiplet. The inherent viscosities were determined at 0.5 g/dL concentration using Tamson TV-2000 viscometer at 30 °C. Gel permeation chromatographic (GPC) analysis was carried out on a Waters chromatography unit interfaced with a Waters 2410 refractive index detector. Two Waters 5 μm Styragel HR-2 and HR-4 columns (7.8 mm ID × 300 mm) were connected in series with NMP as the eluent at a flow rate of 0.5 mL/min at 40 °C and were calibrated with polystyrene standards. Thermogravimetric analysis (TGA) was conducted with a PerkinElmer Pyris 1 TGA. Experiments were carried out on ~6–8 mg film samples heated in flowing nitrogen or air (flow rate = 20 cm^3/min) at a heating rate of 20 °C/min. Differential scanning calorimetry (DSC) analyses were performed on a PerkinElmer Pyris 1 DSC at a scan rate of 10 °C/min in flowing nitrogen (20 cm^3/min). Electrochemistry was performed with a CH Instruments 611B electrochemical analyzer. Voltammograms were presented with the positive potential pointing to the left and with increasing anodic currents pointing downward. Cyclic voltammetry (CV) was conducted with a three-electrode cell in which ITO (polymer films area *ca.* 0.5 cm × 1.1 cm) was used as a working electrode. A platinum wire was used as an auxiliary electrode. All cell potentials were taken by using a homemade Ag/AgCl, KCl (sat.) reference electrode.

Fabrication and Measurement of the Memory Device

The memory device was fabricated with the configuration of indium tin oxide (ITO)/polymer/Al as shown in Figure 1. The ITO glass used for memory device was cleaned by ultrasonication with water, acetone, and isopropanol each for 15 min. A DMAc solution of **PI** or **PA** (15–30 mg/mL) was first filtered through 0.45 μm pore size of PTFE membrane syringe filter. Then, 250 μL of the filtered solution was spin-coated onto the ITO glass at a rotation rate of 1000 rpm for 60 s and kept at 100 °C for 10 min under nitrogen. The thickness of thin films was determined by alpha-step profilometer. A 300-nm-thick Al top electrode was thermally evaporated through the shadow mask (recorded device units of 0.5 × 0.5 mm^2) at a pressure of 10^{-7} Torr with a uniform depositing rate of 3–6 Å/s. The electrical characterization of the memory device was performed by a Keithley 4200-SCS semiconductor parameter analyzer equipped with a Keithely 4205-PG2 arbitrary waveform pulse generator. ITO was used as common electrode and Al was the electrode for applying voltage during the sweep. All the electronic measurements were performed in a glove box.

Molecular Simulation

Molecular simulations in this study were carried out with the Gaussian 09 program package. Equilibrium ground state geometry and electronic properties of basic unit of **PI** or **PA** were optimized by the density functional theory (DFT) method at the B3LYP level of theory (Becke's style three-parameter DFT using the Lee–Yang–Parr correlation functional) with the 6-31G(d) basic set.

RESULTS AND DISCUSSION

Polymer Synthesis and Characterization

The $(OMe)_2$TPPA-based new **PI** was prepared by the reaction of diamine (**1**) with a commercially available dianhydride 6FDA (**3**) in NMP at room temperature to obtain the precursor poly(amic acid), followed by chemical imidization (Scheme 1). The resulting polyimide having high molecular weight and could afford flexible and tough film with reddish color (Scheme 1) due to the charge-transfer behavior between the electron-donating TPPA and the electron-accepting phthalimide units. The GPC analysis data of the polyimide are summarized in Supporting Information Table S1, and the formation of polyimide was confirmed by IR spectroscopy showing characteristic imide absorption bands at around 1782 (symmetrical C= O), 1725 (symmetrical C=O), 1380 (C —N), and 741 cm^{-1} (imide ring deformation; Supporting Information Fig. S1). Chemical structures of the **PA**

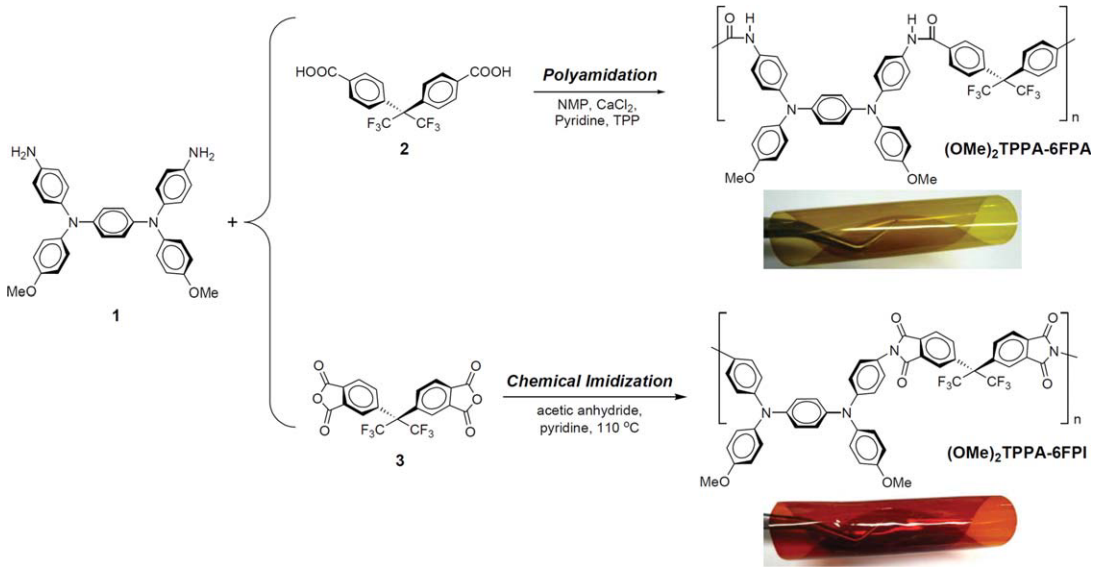

SCHEME 1 Polyamide and polyimide were prepared by polyamidation and two-step chemical imidization, respectively. The photographs show appearance of the flexible films (thickness: ~40 μm).

and **PI** are confirmed by ^{1}H NMR, and the results are shown in Supporting Information Figures S2 and S3. (DMSO-d_6, δ, ppm): **PA** 3.71 (s, 6H, —OCH_3), 6.84 (m, 12H), 6.99 (d, 4H), 7.48 (d, 4H), 7.62 (d, 4H), 7.99 (d, 4H), 10.33 (s, 2H, NH) **PI** 3.70 (s, 6H, —OCH_3), 6.92 (m, 12H), 7.08 (d, 4H), 7.20 (d, 4H), 7.78 (s, 2H), 7.89 (d, 2H), 8.09 (d, 2H), 10.33 (s, 2H, NH). Synthesis and characterization of **PA** have been described previously.[11(b)] Solubility behavior of **PI** was investigated, and the results are listed in Supporting Information Table S2. The detailed information is described in Supporting Information. The thermal properties of the polyimide **PI** and the polyamide **PA** are summarized in Table 1. Typical TGA and DSC curves of **PI** and **PA** in both air and nitrogen atmospheres are shown in Figure 2. The 10% weight-loss temperatures of **PI** in nitrogen and air were recorded as 530 and 545 °C, respectively (535 and 520 °C for **PA**, respectively). The amount of carbonized residue (char yield) of **PI** in nitrogen atmosphere was 61% at 800 °C and 65% for **PA**, which could be ascribed to their high aromatic content.

TABLE 1 Thermal Properties of Polymers

Polymer[a]	T_g[b] (°C)	T_d^5 (°C)[c]		T_d^{10} (°C)[c]		R_{w800} (%)[d]
		N_2	Air	N_2	Air	
$(OMe)_2$TPPA-6FPA	245	500	475	535	520	65
$(OMe)_2$TPPA-6FPI	287	500	495	530	545	61

[a] The polymer film samples were heated at 300 °C for 1 h before all the thermal analyses.
[b] Midpoint temperature of baseline shift on the second DSC heating trace (rate: 20 °C/min) of the sample after quenching from 400 °C to 50 °C (rate: 200 °C/min) in nitrogen.
[c] Temperature at which 5% and 10% weight loss occurred, respectively, was recorded by TGA at a heating rate of 20 °C/min and a gas flow rate of 20 cm^3/min.
[d] Residual weight percentages at 800 °C under nitrogen flow.

Optical and Electrochemical Properties

The optical and electrochemical properties of $(OMe)_2$TPPA-based polyamide and polyimide are summarized in Table 2. The optical energy band gap (E_g) of **PA** and **PI** estimated from the onset optical absorbance is 2.99 and 2.45 eV, respectively. The larger E_g of **PA** than **PI** was resulted from the less electron-withdrawing amide linkage in polyamide than the phthalimide unit in polyimide. The electrochemical behavior of these two polymers was investigated by CV conducted by film cast on an ITO-coated glass substrate as the working electrode in dry acetonitrile (CH_3CN) containing 0.1 M of TBAP as an electrolyte under nitrogen atmosphere. The typical cyclic voltammograms for **PA** and **PI** are shown in Figure 3 for comparison. There are two reversible oxidation redox couples at $E_{1/2}$ values of 0.55 (E_{onset} = 0.44) and

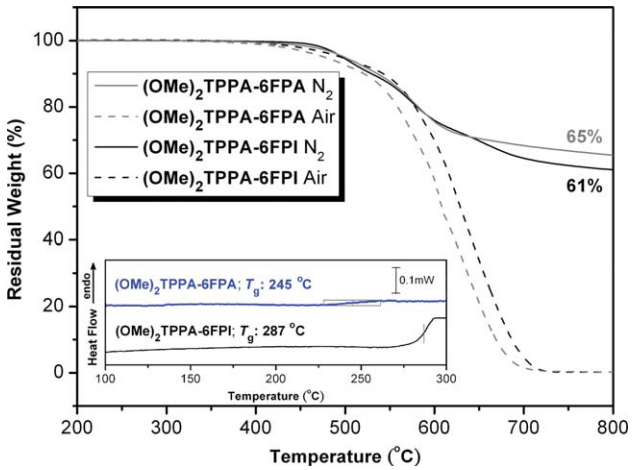

FIGURE 2 TGA thermograms and DSC traces of **$(OMe)_2$TPPA-6FPA** and **$(OMe)_2$TPPA-6FPI**. [Color figure can be viewed in the online issue, which is available at wileyonlinelibrary.com.]

TABLE 2 Redox Potentials and Energy Levels of Polymers

Polymer	UV–Vis Absorption of the Polymer Films (nm)		Oxidation Potential (V)					
			$E_{1/2}$[a]					
	λ_{max}	λ_{onset}	1st	2nd	E_{onset}	E_g[b] (eV)	HOMO[c] (eV)	LUMO (eV)
$(OMe)_2$TPPA-6FPA	308	415	0.55	0.91	0.44	2.99	4.88	1.89
$(OMe)_2$TPPA-6FPI	303	506	0.72	1.01	0.62	2.45	5.06	2.61

[a] $E_{1/2}$ (average potential of the redox couple peaks versus Ag/AgCl in CH_3CN).
[b] The data were calculated from polymer films by the equation: $E_g = 1240/\lambda_{onset}$ (energy gap between HOMO and LUMO).
[c] The HOMO energy levels were calculated from CV and were referenced to ferrocene (4.8 eV; onset = 0.36 V).

0.91 V for polyamide, and 0.72 (E_{onset} = 0.62) and 1.01 V for polyimide in the oxidative scan. The redox potentials of the polymers as well as their respective HOMO and LUMO are summarized in Table 2. The HOMO energy levels of **PA** and **PI** estimated from the onset of their oxidation in CV experiments were 4.88 and 5.06 eV, respectively (on the basis of ferrocene/ferrocenium 4.8 eV below the vacuum level with E_{onset} = 0.36 V[12]).

Memory Device Characteristics of These Polymers

The memory behaviors of **PI** and **PA** were demonstrated by the current–voltage (*I–V*) characteristics of an ITO/polymer/Al sandwich device as shown in Figure 1. Within the sandwich device, polymer film was used as an active layer between Al and ITO as the top and bottom electrodes. To exclude the effect of the polymer film thickness on memory properties, a standard thickness (50 nm) was used without specific mention. Figure 4 depicts the *I–V* results of **PI**, which were measured with a compliance current of 0.01 A. During the first positive sweep from 0 V to 6 V, the device stayed in the low-conductivity (OFF) state with a current range 10^{-13} to 10^{-14} A, which means that the positive applied voltage could not switch the memory device on. On the contrary, the current increased abruptly from 10^{-13} to 10^{-14} to 10^{-5} A (high-conductivity state) at the threshold voltage of −4.6 V in the second negative sweep, indicating the transition from the OFF state to high-conductivity (ON) state. In a memory device, this OFF-to-ON transition can be defined as a "writing" process. The device remained in the ON state during the subsequent negative scan (the third sweep) and then positive scan (the fourth sweep). The memory device could not be reset to the initial OFF state by applying a reverse scan

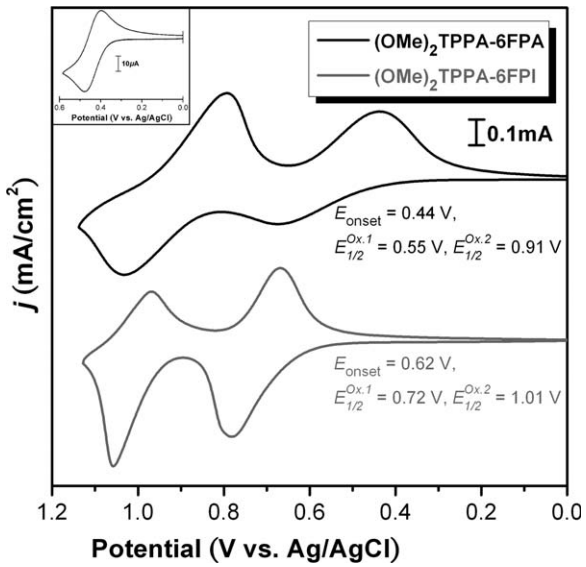

FIGURE 3 Cyclic voltammetric diagrams of polymer **$(OMe)_2$TPPA-6FPI** and **$(OMe)_2$TPPA-6FPA** films on an ITO-coated glass substrate over cyclic scans and ferrocene (inset) in 0.1 M TBAP/CH_3CN at a scan rate of 50 mV/s.

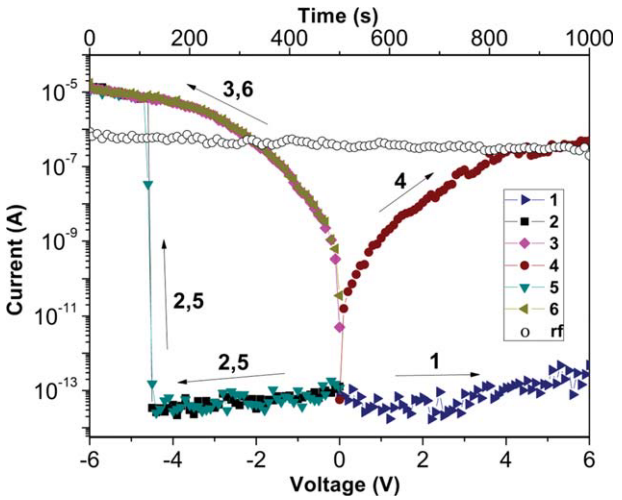

FIGURE 4 Current–voltage (*I–V*) characteristics of the ITO/**$(OMe)_2$TPPA-6FPI** (50 nm)/Al memory device. (The fifth sweep was conducted about 15 s after turning off the power, and the rf trace was measured by a refreshing voltage pulse of −2 V every 5 s for 1000 s.) [Color figure can be viewed in the online issue, which is available at wileyonlinelibrary.com.]

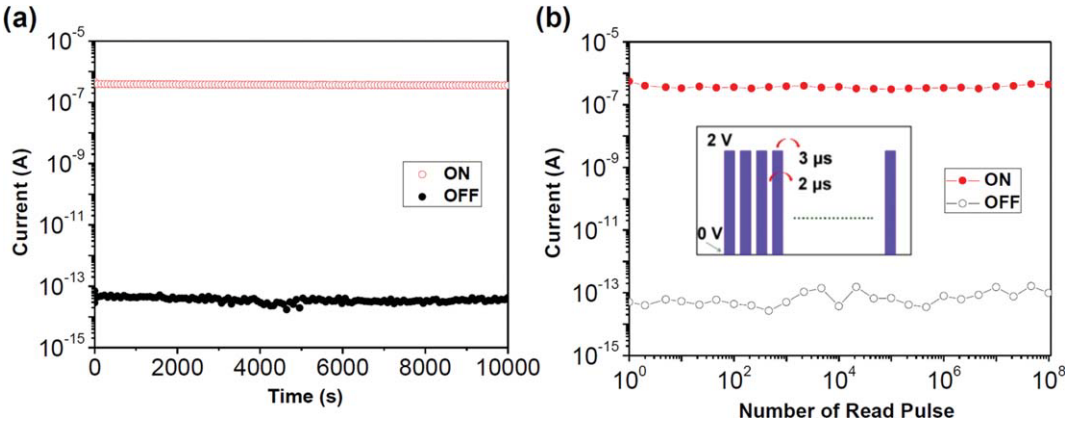

FIGURE 5 a: Effect of operation time on the ON and OFF states of the ITO/**$(OMe)_2$TPPA-6FPI** (50 nm)/Al device with a continuous −2 V. b: Stimulus effect of read pulses on the ON and OFF states of the **$(OMe)_2$TPPA-6FPI** (50 nm) device. The inset shows the pulse shapes of the measurement. [Color figure can be viewed in the online issue, which is available at wileyonlinelibrary.com.]

implying the nonerasable behavior. The fifth sweep was conducted after turning off the power for about 15 s; and found that the ON state had relaxed to the steady OFF state. It suggests that the ON state could be retained for a short period after the removal of applied voltage and then relaxed to the initial OFF state eventually. The device could also be reprogrammed by starting from the OFF state to the ON state again with an accurate threshold voltage of −4.6 V in the fifth sweep, and kept in the ON state in the subsequent sixth sweep. The fifth and sixth sweeps were conducted to confirm that the memory device is rewritable. The very short retention time of the ON state indicates that the memory device showed volatile DRAM property, and this volatile ON state could be maintained by a refreshing voltage pulse of −2 V (1 ms duration) every 5 s for 1000 s (named the rf trace in Fig. 4). To further investigate the stability of the DRAM characteristic, ON/OFF current ratio and retention time were measured and are depicted in Figure 5. The effect of operation time on the ON and OFF states of the ITO/**PI**/Al device with a continuous −2 V is represented in Figure 5(a). The memory device was initially switched to a high (ON) or low (OFF) conductivity state, respectively, and then applying a constant stress of −2 V. There was no obvious degradation in current could be observed at both ON and OFF states for at least 10^4 s during the readout test. Furthermore, the ON and OFF state were also stable up to 10^8 read pulses of −2 V as shown in Figure 5(b). (The pulse period and width are 3 and 2 μs, respectively, as shown in the inset.)

The *I*–*V* characteristics of the ITO/polymer/Al sandwich device were also used to describe the memory properties of **PA** as depicted in Figure 6. The device based on the polyamide could not be switched to the ON state and stayed in the OFF state with a current range 10^{-13} to 10^{-14} in the first positive sweep up to 6 V. However, a sharp increase in the current could be observed at −3.3 V during the second negative sweep, indicating that the device undergoes an electrical transition from the OFF state to the ON state (writing process). The device also remained in the ON state during the subsequent negative (the third sweep) and positive scans (the fourth sweep). Thus, this **PA** memory device could not be reset to the initial OFF state by the introduction of a reverse scan and is thus nonerasable. Interestingly, the device of **PA** still maintained in the ON state after turning off the power for a longer period of time than in polyimide. The fifth sweep was conducted after turning off the power for about 10 min; it was found that the ON state had relaxed to the steady OFF state without an erasing process. During the fifth sweep, the device could be switched to the ON state again at the threshold voltage of −3.1 V, and the sixth sweep was conducted to make sure the device could open to the ON state again. The longer retention time at the ON state yet volatile, as well as the randomly accessible ON and OFF states in each ITO/**PA**/Al device are similar to the data remanence behavior of SRAM.[8(i)] The effect of operation time on the ON and OFF states of the ITO/**PA**/Al device with

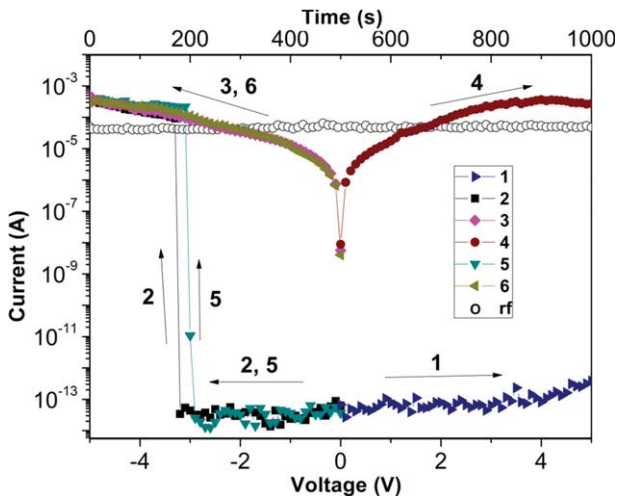

FIGURE 6 Current–voltage (*I*–*V*) characteristics of the ITO/**$(OMe)_2$TPPA-6FPA** (50 nm)/Al memory device. (The fifth sweep was conducted about 10 min after turning off the power, and the rf trace was measured by a refreshing voltage pulse of −2 V every 5 s for 1000 s.)

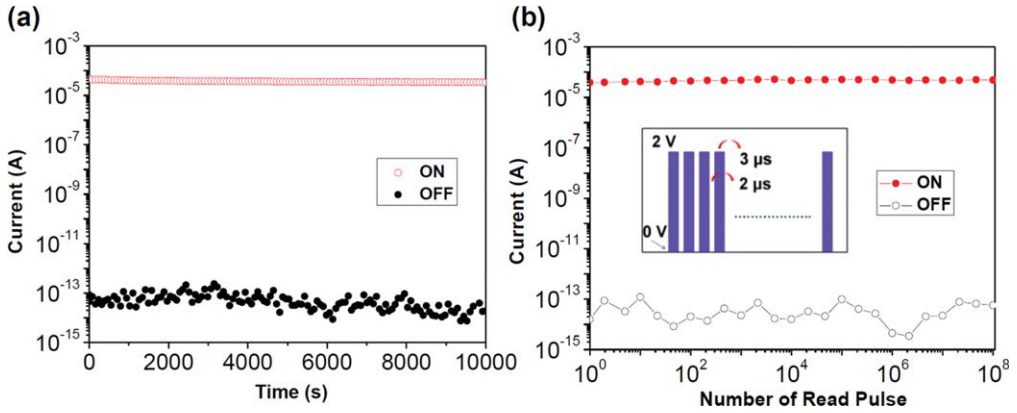

FIGURE 7 a: Effect of operation time on the ON and OFF states of the ITO/**$(OMe)_2$TPPA-6FPA** (50 nm)/Al device with a continuous −2 V. b: Stimulus effect of read pulses on the ON and OFF states of the **$(OMe)_2$TPPA-6FPA** (50 nm) device. The inset shows the pulse shapes of the measurement. [Color figure can be viewed in the online issue, which is available at wileyonlinelibrary.com.]

continuous −2 V was investigated as shown in Figure 7(a), and no obvious degradation in current could be observed at both ON and OFF states for at least 10^4 s in the readout test. In addition, the excellent stability of this polyamide type memory device was also confirmed by read pulses test of −2 V for 10^8 cycles as depicted in Figure 7(b).

Theoretical Analysis and Switching Mechanism

To get more insight into the different memory behavior of the present **PI** and **PA** device, molecular simulation on the basic unit was carried out by DFT/B3LYP/6-31G(d) with the Gaussian 09 program. The charge density isosurfaces of the basic unit and the most energetically favorable geometry were summarized in Figure 8. For both **PI** and **PA** systems, the HOMO is located mainly at the electron-donating TPPA moieties, whereas LUMO is located at the electron-withdrawing phthalimide units for **PI** and at the amide linkage and adjacent phenyl ring for **PA**. In **PI** system, the location of LUMO5 is at the TPPA moieties, whereas the three intermediate LUMOs (LUMO2, LUMO3, and LUMO4) are distributed around phthalimide units. According to the literatures,[8(b,h,i,k)] when the applied electric fields reach the switching-on voltage, some electrons at the HOMO accumulate energy and transit to the LUMO5 with the highest probability because of overlapping of the HOMO and LUMO5 resulting in an excited state. In addition, electrons at the HOMO can also be excited to the three intermediate LUMOs with lower energy barrier. Thus, charge transfer can occur through several courses to form the conductive charge-transfer complexes: indirectly from the LUMO5 to the intermediate LUMOs and then to the LUMO, or from the intermediate LUMOs to the LUMO, and directly from the HOMO to the LUMO. When the intra- or intermolecular charge transfer occurring by the applied electric field, the generating holes can be delocalized to the conjugated TPPA moieties resulting in an open channel in the HOMO of **PI** for the charge carriers (holes) to migrate through. Therefore, the current increases rapidly and the memory device can be switched to the high-conductivity state (ON state).

Comparing with the simulation result of **PI**, the corresponding **PA** exhibited different LUMO charge density isosurfaces. As shown in Figure 8, charge location of LUMO4 is mainly on the TPPA units for **PA**, while distributed around the phthalimide moieties for **PI**. The intermediate LUMOs of **PA** are less than those of **PI** implying the higher probability of indirect charge transfer from HOMO to LUMO4 in **PA**. Meanwhile, the fewer intermediate LUMOs also lead to form the

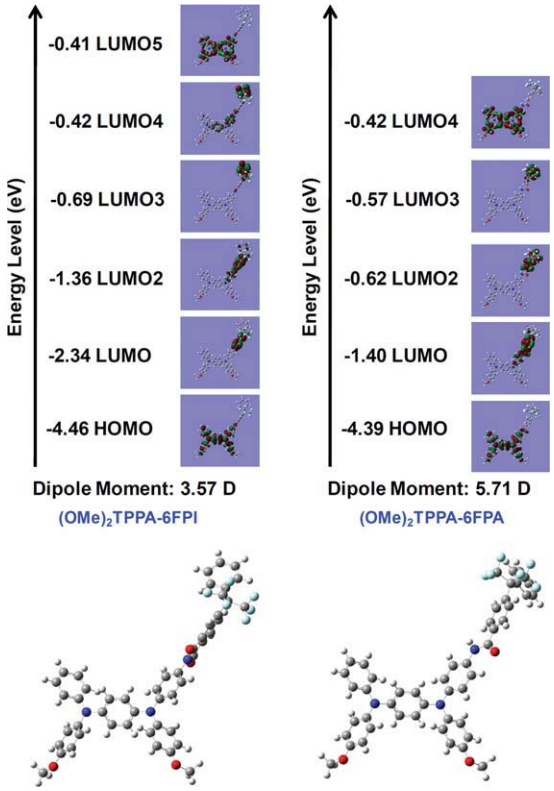

FIGURE 8 Calculated molecular orbitals and corresponding energy levels of the basic units (BU) for polyimide and polyamide, respectively. [Color figure can be viewed in the online issue, which is available at wileyonlinelibrary.com.]

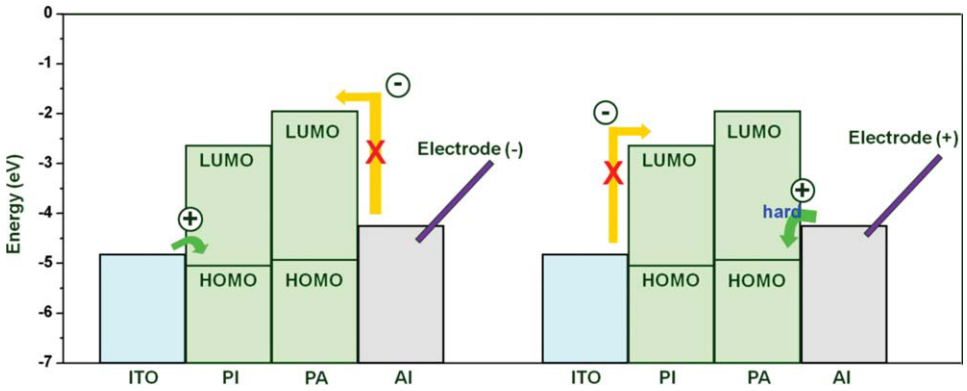

FIGURE 9 LUMO and HOMO energy levels of **$(OMe)_2$TPPA-6FPI** and **$(OMe)_2$TPPA-6FPA** along with the work function of the electrodes. [Color figure can be viewed in the online issue, which is available at wileyonlinelibrary.com.]

conductive charge-transfer complexes more easily, which is one of the reasons that **PA** revealed lower switching-on voltage than **PI**. Furthermore, the theoretical dipole moments of these two polymers were also calculated by Gaussian 09 and represented at the bottom of Figure 8. The higher dipole moment of **PA** (5.71 D) than that of **PI** (3.57 D) leads to a more stable CT complex;[8(c,d,i,j)] thus, **PA** could show unique SRAM but **PI** only revealed more volatile DRAM behaviors. The difference of linkage conformation also plays an important role to the DRAM and SRAM properties of **PI** and **PA**, respectively. The phthalimide moieties of **PI** form a new plane (dihedral angles 179.5°) with adjacent phenyl ring that favor the occurring of back CT; however, the conformation of phenyl ring with amide linkage is not a planar structure which may block the occurring of back CT as shown in Figure 8, resulting in longer retention time of **PA** system after removing applied power (SRAM). The HOMO and LUMO energy levels of these two polymers calculated from CV measurements and the optical band gaps are illustrated in Figure 9 along with the work functions of the Al and ITO electrodes. When the negative sweep was conducted, the hole injected from the bottom electrode ITO to the HOMO of polymer;[4(i),13] thus, the higher energy level HOMO of **PA** effectively leads to a lower energy barrier, resulting in lower switching-on voltage of **PA** than **PI**. On the contrary, hole is hard to be injected from the top electrode Al into the HOMO of these polymers because of the larger energy gap between the work function of Al (−4.2 eV) and HOMO of the polymers than in ITO (−4.8 eV); thus, the memory device could not be switched to the ON state during the positive sweep.

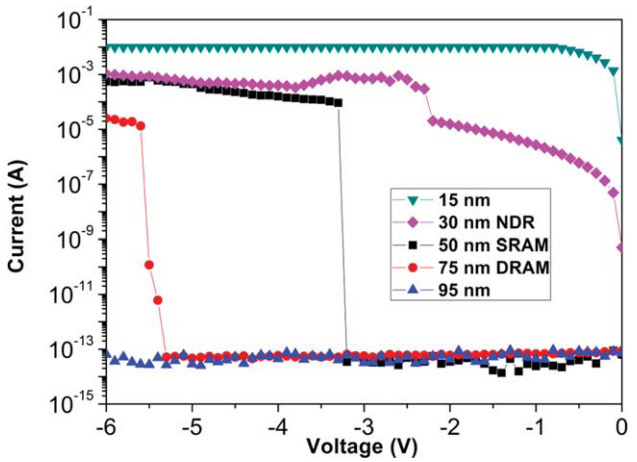

FIGURE 10 Effect of thickness on memory properties of **$(OMe)_2$TPPA-6FPA**. [Color figure can be viewed in the online issue, which is available at wileyonlinelibrary.com.]

Thickness Effect of the Polyamide on Memory Properties

In addition to the aforementioned interesting and excellent memory characteristics, we also prepared devices of **PA** films with various thicknesses (15, 30, 50, 75, and 95 nm) and investigated their memory performance. The effect of polymer film thickness on memory properties of **PA** is depicted in Figure 10. First of all, the 15-nm thick **PA** films always exhibited high conductivity close to the compliance current of 10^{-2} A, which is the limit of the semiconductor analyzer used in this study. Then, the thickness of **PA** films was increased to 30 nm, the resulted devices showed a negative differential resistance (NDR) property during the switching-on process, and the ON state current also closed to 10^{-2} A. According to previous literature,[8(g),14] the high current of the ON state and the NDR phenomenon in 15 and 30 nm thickness for the polyamide device were resulted from the filament formation of Al atom. The polymer devices stayed in the OFF state both in negative and positive sweep when the thickness of the polymer film was increased to 95 nm. The memory properties of **PA** with 50 nm thickness revealed SRAM characteristic and high ON/OFF current ratio as afore described, while exhibited spectacular DRAM property and higher switching-on voltage (−5.3 V) in 75 nm. The different memory behavior between 50 and 75 nm is interesting and worth to be further investigated because the switching mechanism may be resulting both from the space charge limited current (SCLC) and charge-transfer effect in one case.

CONCLUSIONS

The new functional **PI** has been successfully synthesized for memory device application. The memory devices with the configuration of ITO/**PI**/Al exhibited distinct volatile memory characteristics of DRAM, whereas the device of **PA** revealed different volatile SRAM property. To the best of our knowledge, there is no polyamide memory material reported to date. The switching mechanism of the memory devices was further investigated by molecular simulation, the **PA** structure with higher dipole moment and nonplanar linkage

resulted in specific SRAM property which was different from **PI** system. In addition, the higher HOMO energy level and fewer intermediate LUMOs of **PA** showed a lower switching-on voltage than **PI** system because of the lower energy barrier between HOMO and work function of bottom electrode ITO and higher probability of indirectly charge transfer from HOMO to LUMO4. The memory devices derived from these two novel high-performance polymers showed excellent stability with a long retention time of 10^4 s by applying continuous -2 V. These results demonstrate the further advantage of functional aromatic polyamides for memory device application.

The authors gratefully acknowledge the financial support of this research through the National Science Council of Taiwan. C. W. Lu at the Instrumentation Center, National Taiwan University, for CHNS (EA) analysis experiments is also acknowledged.

REFERENCES AND NOTES

1 (a) Friend, R. H.; Gymer, R. W.; Holmes, A. B.; Burroughes, J. H.; Marks, R. N.; Taliani, C.; Bradley, D. D. C.; Dos Santos, D. A.; Bredas, J. L.; Logdlund, M.; Salaneck, W. R. Nature 1999, 397, 121–128; (b) Lee, K.; Kim, J. Y.; Park, S. H.; Kim, S. H.; Cho, S.; Heeger, A. J. Adv Mater 2007, 19, 2445–2449; (c) Shao, Y.; Bazan, G. C.; Heeger, A. J. Adv Mater 2008, 20, 1191–1193; (d) Shao, Y.; Gong, X.; Heeger, A. J.; Liu, M.; Jen, A. K. Y. Adv Mater 2009, 21, 1972–1975.

2 (a) Sirringhaus, H.; Tessler, N.; Friend, R. H. Science 1998, 280, 1741–1744; (b) Yamamoto, T.; Kokubo, H.; Kobashi, M.; Sakai, Y. Chem Mater 2004, 16, 4616–4618; (c) Chua, L. L.; Zaumseil, J.; Chang, J. F.; Ou, E. C. W.; Ho, P. K. H.; Sirringhaus, H.; Friend, R. H. Nature 2005, 434, 194–199; (d) Babel, A.; Zhu, Y.; Cheng, K. F.; Chen, W. C.; Jenekhe, S. A. Adv Funct Mater 2007, 17, 2542–2549; (e) Morana, M.; Koers, P.; Waldauf, C.; Koppe, M.; Muehlbacher, D.; Denk, P.; Scharber, M.; Waller, D.; Brabec, C. Adv Funct Mater 2007, 17, 3274–3283; (f) Morana, M.; Wegscheider, M.; Bonanni, A.; Kopidakis, N.; Shaheen, S.; Scharber, M.; Zhu, Z.; Waller, D.; Gaudiana, R.; Brabec, C. Adv Funct Mater 2008, 18, 1757–1766; (g) Yan, H.; Chen, Z. H.; Zheng, Y.; Newman, C.; Quinn, J. R.; Dotz, F.; Kastler, M.; Facchetti, A. Nature 2009, 457, 679–687; (h) Tsai, J. H.; Lee, W. Y.; Chen, W. C.; Yu, C. Y.; Hwang, G. W.; Ting, C. Chem Mater 2010, 22, 3290–3299.

3 (a) Yu, G.; Gao, J.; Hummelen, J. C.; Wudl, F.; Heeger, A. J. Science 1995, 270, 1789–1791; (b) Brabec, C. J.; Sariciftci, N. S.; Hummelen, J. C. Adv Funct Mater 2001, 11, 15–26; (c) Li, G.; Shrotriya, V.; Huang, J. S.; Yao, Y.; Moriarty, T.; Emery, K.; Yang, Y. Nat Mater 2005, 4, 864–868; (d) Chen, M. H.; Hou, J.; Hong, Z.; Yang, G.; Sista, S.; Chen, L. M.; Yang, Y. Adv Mater 2009, 21, 4238–4242; (e) Hou, J. H.; Chen, T. L.; Zhang, S. Q.; Huo, L. J.; Sista, S.; Yang, Y. Macromolecules 2009, 42, 9217–9219; (f) Kumar, A.; Liao, H. H.; Yang, Y. Org Electron 2009, 10, 1615–1620; (g) Huo, L. J.; Hou, J. H.; Zhang, S. Q.; Chen, H. Y.; Yang, Y. Angew Chem Int Ed 2010, 49, 1500–1503; (h) Sista, S.; Hong, Z. R.; Park, M. H.; Xu, Z.; Yang, Y. Adv Mater 2010, 22, E77–E80.

4 (a) Yang, Y.; Ouyang, J.; Ma, L. P.; Tseng, R. J. H.; Chu, C. W. Adv Funct Mater 2006, 16, 1001–1014; (b) Baek, S.; Lee, D.; Kim, J.; Hong, S. H.; Kim, O.; Ree, M. Adv Funct Mater 2007, 17, 2637–2644; (c) Ling, Q. D.; Liaw, D. J.; Teo, E. Y. H.; Zhu, C. X.; Chan, D. S. H.; Kang, E. T.; Neoh, K. G. Polymer 2007, 48, 5182–5201; (d) Ling, Q. D.; Liaw, D. J.; Zhu, C. X.; Chan, D. S. H.; Kang, E. T.; Neoh, K. G. Prog Polym Sci 2008, 33, 917–978; (e) Lee, T. J.; Park, S.; Hahm, S. G.; Kim, D. M.; Kim, K.; Kim, J.; Kwon, W.; Kim, Y.; Chang, T.; Ree, M. J Phys Chem C 2009, 113, 3855–3861; (f) Liu, G.; Ling, Q. D.; Teo, E. Y. H.; Zhu, C. X.; Chan, D. S. H.; Neoh, K. G.; Kang, E. T. ACS Nano 2009, 3, 1929–1937; (g) Fang, Y. K.; Liu, C. L.; Li, C. X.; Lin, C. J.; Mezzenga, R.; Chen, W. C. Adv Funct Mater 2010, 20, 3012–3024; (h) Park, S.; Lee, T. J.; Kim, D. M.; Kim, J. C.; Kim, K.; Kwon, W.; Ko, Y. G.; Choi, H.; Chang, T.; Ree, M. J Phys Chem B 2010, 114, 10294–10301; (i) Zhuang, X. D.; Chen, Y.; Liu, G.; Zhang, B.; Neoh, K. G.; Kang, E. T.; Zhu, C. X.; Li, Y. X.; Niu, L. J. Adv Funct Mater 2010, 20, 2916–2922.

5 Stikeman, A. Technol Rev 2002, 31.

6 Lee, C.; Kim, I.; Shin, H.; Kim, S.; Cho, J. Langmuir 2009, 25, 11276–11281.

7 (a) Lin, H. T.; Pei, Z. W.; Chen, J. R.; Hwang, G. W.; Fan, J. F.; Chan, Y. J. IEEE Electr Device L 2007, 28, 951–953; (b) Laiho, A.; Majumdar, H. S.; Baral, J. K.; Jansson, F.; Osterbacka, R.; Ikkala, O. Appl Phys Lett 2008, 93, 203309-1–203309-3; (c) Liu, G.; Ling, Q. D.; Kang, E. T.; Neoh, K. G.; Liaw, D. J.; Chang, F. C.; Zhu, C. X.; Chan, D. S. H. J. Appl Phys 2007, 102, 024502-1–024502-8; (d) Tseng, R. J.; Huang, J. X.; Ouyang, J.; Kaner, R. B.; Yang, Y. Nano Lett 2005, 5, 1077–1080; (e) Ouyang, J. Y.; Chu, C. W.; Tseng, R. J. H.; Prakash, A.; Yang, Y. Proc. IEEE 2005, 93, 1287–1296; (f) Ouyang, J. Y.; Chu, C. W.; Szmanda, C. R.; Ma, L. P.; Yang, Y. Nat Mater 2004, 3, 918–922.

8 (a) Cheng, S. H.; Hsiao, S. H.; Su, T. X.; Liou, G. S. Macromolecules 2005, 38, 307–316; (b) Ling, Q. D.; Chang, F. C.; Song, Y.; Zhu, C. X.; Liaw, D. J.; Chan, D. S. H.; Kang, E. T.; Neoh, K. G. J Am Chem Soc 2006, 128, 8732–8733; (c) Hahm, S. G.; Choi, S.; Hong, S. H.; Lee, T. J.; Park, S.; Kim, D. M.; Kwon, W. S.; Kim, K.; Kim, O.; Ree, M. Adv Funct Mater 2008, 18, 3276–3282; (d) Hahm, S. G.; Choi, S.; Hong, S. H.; Lee, T. J.; Park, S.; Kim, D. M.; Kim, J. C.; Kwon, W.; Kim, K.; Kim, M. J.; Kim, O.; Ree, M. J Mater Chem 2009, 19, 2207–2214; (e) Kim, D. M.; Park, S.; Lee, T. J.; Hahm, S. G.; Kim, K.; Kim, J. C.; Kwon, W.; Ree, M. Langmuir 2009, 25, 11713–11719; (f) Kim, K.; Park, S.; Hahm, S. G.; Lee, T. J.; Kim, D. M.; Kim, J. C.; Kwon, W.; Ko, Y. G.; Ree, M. J Phys Chem B 2009, 113, 9143–9150; (g) Lee, T. J.; Chang, C. W.; Hahm, S. G.; Kim, K.; Park, S.; Kim, D. M.; Kim, J.; Kwon, W. S.; Liou, G. S.; Ree, M. Nanotechnology 2009, 20, 135204; (h) Liu, Y. L.; Ling, Q. D.; Kang, E. T.; Neoh, K. G.; Liaw, D. J.; Wang, K. L.; Liou, W. T.; Zhu, C. X.; Chan, D. S. H. J Appl Phys 2009, 105, 044501-1–044501-9; (i) Liu, Y. L.; Wang, K. L.; Huang, G. S.; Zhu, C. X.; Tok, E. S.; Neoh, K. G.; Kang, E. T. Chem Mater 2009, 21, 3391–3399; (j) You, N. H.; Chueh, C. C.; Liu, C. L.; Ueda, M.; Chen, W. C. Macromolecules 2009, 42, 4456–4463; (k) Kuorosawa, T.; Chueh, C. C.; Liu, C. L.; Higashihara, T.; Ueda, M.; Chen, W. C. Macromolecules 2010, 43, 1236–1244; (l) Wang, K. L.; Liu, Y. L.; Lee, J. W.; Neoh, K. G.; Kang, E. T. Macromolecules 2010, 43, 7159–7164.

9 (a) Majumdar, H. S.; Bandyopadhyay, A.; Bolognesi, A.; Pal, A. J. J Appl Phys 2002, 91, 2433–2437; (b) Teo, E. Y. H.; Ling, Q. D.; Song, Y.; Tan, Y. P.; Wang, W.; Kang, E. T.; Chan, D. S. H.; Zhu, C. Org Electron 2006, 7, 173–180.

10 (a) Huang, L. T.; Yen, H. J.; Chang, C. W.; Liou, G. S. J Polym Sci Part A: Polym Chem 2010, 48, 4747–4757; (b) Hsiao, S. H.; Liou, G. S.; Wang, H. M. J Polym Sci Part A: Polym Chem 2009, 47, 2330–2343; (c) Chang, H. W.; Lin, K. H.; Chueh, C. C.; Liou, G. S.; Chen, W. C. J Polym Sci Part A: Polym Chem 2009, 47, 4037–4050; (d) Liou, G. S.; Yen, H. J.; Chiang, M. C. J Polym Sci Part A: Polym Chem 2009, 47, 5378–5385.

11 (a) Chang, C. W.; Liou, G. S.; Hsiao, S. H. J Mater Chem 2007, 17, 1007–1015; (b) Yen, H. J.; Liou, G. S. Chem Mater 2009, 21, 4062–4070.

12 Gritzner, G.; Kutta, J. Pure Appl Chem 1984, 56, 461.

13 Ling, Q. D.; Song, Y.; Lim, S. L.; Teo, E. Y. H.; Tan, Y. P.; Zhu, C. X.; Chan, D. S. H.; Kwong, D. L.; Kang, E. T.; Neoh, K. G. Angew Chem Int Ed 2006, 45, 2947–2951.

14 (a) You, Y. T.; Wang, M. L.; Xuxie, H. N.; Wu, B.; Sun, Z. Y.; Hou, X. Y. Appl Phys Lett 2010, 97, 233301–1–233301–3; (b) Tang, W.; Shi, H. Z.; Xu, G.; Ong, B. S.; Popovic, Z. D.; Deng, J. C.; Zhao, J.; Rao, G. H. Adv Mater 2005, 17, 2307–2311.